A Unified Approach for Inverse Problem in EEG and Brain Connectivity with Application to Epilepsy. A Proof of Concept Study.

Ahmad Karfoul
Univ Rennes, Inserm, LTSI - UMR 1099
F-35000 Rennes, France
ahmad.karfoul@univ-rennes.fr

Amar Kachenoura
Univ Rennes, Inserm, LTSI - UMR 1099
F-35000 Rennes, France
amar.kachenoura@univ-rennes.fr

Laurent Albera
Univ Rennes, Inserm, LTSI - UMR 1099
F-35000 Rennes, France
laurent.albera@univ-rennes.fr

***Abstract*—The analysis of brain source connectivity using scalp EEG is conventionally performed in two successive steps: solving the EEG inverse problem then estimating brain connectivity. Such sequential manner is sub-optimal since the results of the latter step are highly subject to the quality of the source localization one. To address this limitation, a proof of concept study on solving the EEG inverse problem and inferring brain functional connectivity in only one single step leading to a new *All-in-One* approach is considered in this paper in the context of drug-resistant epilepsy. Both minimum norm and smoothness on graph assumptions on the target extended epileptic sources are used to restore the identifiability of the ill-posed EEG inverse problem. Preliminary results on realistic simulated surface epileptic EEG signals confirm the potential of the proposed approach.**

***Index Terms*—Inverse problem, EEG, brain connectivity, graph learning, proximal optimization.**

I. Introduction

There is an emerging consensus that the human brain is a complex network of distributed interconnected regions. Thus, the inference and the analysis of brain connectivity are fundamental in neuroscience to understand both normal and pathological brain functions [1] by identifying alterations in brain networks. Brain connectivity is thus crucial to elucidate how neurons and neural networks process information [2]–[4]. A fundamental distinction in connectivity comes from the notions of structural connectivity, functional connectivity and effective connectivity [3], [5], [6]. This study concerns only brain functional connectivity which refers to the statistical dependence measured between the activities of spatially remote regions. Thanks to its many attractive properties such as non-invasiveness and high temporal resolution, ElectroEncephaloGraphy (EEG) is considered as a gold standard to analyse brain activity. High temporal resolution is fundamental not only for an efficient tracking of brain networks but also for detecting their possible alteration in neural disorders cases such as epilepsy typically during interictal and/or ictal periods [7]. Epilepsy is a group of neurological disorders characterized by repetitive seizures which are induced by abnormal excessive or synchronous neuronal activity in certain regions of the brain, known as epileptogenic. When the therapy by surgery is the solution to be adopted, the question is then to identify the epileptogenic network or the Epileptogenic Zone (EZ) which is responsible for the initiation and/or the propagation of epileptic seizures. Identifying this epileptogenic network from surface EEG recordings is typically performed through two successive processing steps, (i) solving the inverse problem in EEG and next (ii) inferring connectivity among localized brain sources using their estimated neural activities. Despite its widespread use, several downsides can be noted in this sequential approach: firstly, the lack of the optimal combination between the source localization method and the connectivity measure for an optimal analysis of brain networks. Authors in [8] has recently addressed this issue in the context of interictal brain networks identification. More precisely, they argued that the combination of the weighted Minimum Norm Estimate (wMNE) algorithm [9] and the Phase Locking Value (PLV) connectivity measure stands for the most relevant source localization-brain connectivity combination. However, despite this interesting results, such a combination is still highly application dependent. Secondly, the reliability of inferring brain connectivity is closely tied to the resolution of the EEG inverse problem. To cope with these aforementioned limitations and motivated by the promising results we recently obtained in the context of epileptic source localization using a steps-coupling strategy [10], a Proof of Concept (POC) study on solving the EEG inverse problem and the inference of brain functional connectivity in only one single step leading to an *All-in-One* (AiO) algorithm is proposed in this paper. More precisely, the inference of brain functional connectivity is formulated here as a graph learning problem [11], [12] for which the activities of the extended epileptic sources are assumed to be smooth signals on graph. In the proposed AiO method, the well-established wMNE algorithm [9], commonly employed for solving the EEG inverse problem, is reexamined. This reevaluation involves integrating the graph learning problem as a regularization term into the ill-posed EEG inverse problem, resulting in the development of the AiOMNE (All-in-One Minimum Norm Estimate-based) method. The proposed approach is evaluated on simulated surface epileptic EEG signals and compared to the classical sequential scheme in terms of source localization accuracy, using both conventional

wMNE and sLORETA [13] algorithms, and brain functional connectivity.

II. Notations and definitions

Throughout this paper, scalars, vectors and matrices are typeset with normal italic lower cases, (e.g., a), bold italic lower cases (e.g., $\boldsymbol{a}$) and bold italic caps (e.g., $\boldsymbol{A}$). Sets are typesets as (e.g., $\mathbb{E}$) and $|\mathbb{E}|$ denotes the cardinal of $\mathbb{E}$. The nth component of a vector $\boldsymbol{a}$ is denoted by a_n and the (i,j)th entry of a matrix $\boldsymbol{A}$ is denoted by $A_{i,j}$, respectively. The Frobenius norm of a matrix and the trasposition operator are denoted by $\|.\|_F$ and $^\intercal$, respectively. $\mathbf{1}_N$ is a N-dimensional vector of ones and † symbolises the Moore–Penrose inverse, respectively,

Definition 1: An undirected weighted graph $\mathcal{G}(\mathbb{V}, \mathbb{E}, \boldsymbol{W})$ is a finite set of vertices (N vertices with $N = |\mathbb{V}|$) that are linked with a set of edges $\mathbb{E}$ with weights (connection strengths) defined in the adjacency matrix $\boldsymbol{W}$.

Definition 2: The adjacency matrix, $\boldsymbol{W}$, associated with the undirected weighted graph $\mathcal{G}(\mathbb{V}, \mathbb{E}, \boldsymbol{W})$ is symmetric and defined as follows:

$$\begin{cases} W_{i,i} = 0, & 1 \leq i \leq N, \\ W_{i,j} \neq 0, & \text{if } V_i \text{ and } V_j \ (i \neq j) \text{ are connected}, \\ W_{i,j} = 0, & \text{otherwise.} \end{cases} \quad (1)$$

Computing graph weights is conventionally performed using functions reflecting some similarity measures (ex. correlations, coherence, phase locking, signal intensity, distance, etc.) among different graph nodes. When no function to compute the latter weights is specified, the Gaussian kernel weighting function is employed (see [14] for extensive details).

Definition 3: A graph signal is a function $f : \mathbb{V} \rightarrow \mathbb{R}$ assigning a real value to each graph vertex.

According to the above definition, the nth sample (component) of a $|\mathbb{V}|$-dimensional graph signal represents the signal value at the nth vertex.

Definition 4: The graph Laplacian matrix, $\boldsymbol{L}$, associated with $\mathcal{G}(\mathbb{V}, \mathbb{E}, \boldsymbol{W})$ is defined as $\boldsymbol{L} = \boldsymbol{D} - \boldsymbol{W}$ with $\boldsymbol{D}$ denoting the graph's degree matrix which is diagonal with entries $D_{i,i} = \sum_{j=1}^{N} W_{i,j}$.

The Laplacian matrix is by construction symmetric positive semi-definite. Hence, it admits an eigenvalue decomposition, $\boldsymbol{L} = \boldsymbol{U}\boldsymbol{\Lambda}\boldsymbol{U}^\intercal$, with non-negative eigenvalues $\lambda_n, 1 \leq n \leq N$. It can be shown that the nth eigenvector in $\boldsymbol{U}$ is a graph Fourier basis vector associated with a frequency (variation of signal values on the graph) that corresponds to the associated nth eigenvalue, λ_n in $\boldsymbol{\Lambda}$ [15].

Definition 5: A smooth signal on a graph $\mathcal{G}$ is a signal that has a slow variation over the graph's vertices.

Assume without loss of generality that the eigenvalues of $\boldsymbol{L}$ are ordered such that $0 \leq \lambda_0 \leq \lambda_1 \leq \cdots \leq \lambda_{max}$, then a graph Fourier representation of the graph signal at frequency λ_n is a smoother graph signal than its representation at frequency λ_{n+1}. Besides, the normalized Laplacian matrix denoted by $\tilde{\boldsymbol{L}}$ where $\tilde{\boldsymbol{L}} = \boldsymbol{D}^{-1/2}\boldsymbol{L}\boldsymbol{D}^{-1/2} = \mathbf{I} - \boldsymbol{D}^{-1/2}\boldsymbol{W}\boldsymbol{D}^{-1/2}$, is widely used in graph theory. The latter matrix inherits all properties enjoyed by the matrix $\boldsymbol{L}$ except that its eigenvalues $\tilde{\lambda}_n, 1 \leq n \leq N$ satisfy $0 \leq \tilde{\lambda}_n \leq 2$. Thus, the normalized graph Laplacian matrix, $\tilde{\boldsymbol{L}}$, is preferable to $\boldsymbol{L}$ since, contrary to the latter matrix, the spectrum of the former is contained in the range $[0, 2]$ [16]. The smoothness of a graph signal $\boldsymbol{x}$ over the given graph is quantified using the Laplacian quadratic form which is defined as follows:

$$\Delta_{\boldsymbol{L}}(\boldsymbol{x}) = \boldsymbol{x}^\intercal \boldsymbol{L}\boldsymbol{x} = \sum_{i,j,i\neq j} W_{i,j}(x(i) - x(j))^2 \quad (2)$$

where the summation is taken over all edges. It becomes evident from equation (2) that the increase in the value of $\Delta_{\boldsymbol{L}}(\boldsymbol{x})$ directly corresponds to a higher degree of signal variation across the graph nodes.

III. Methodology

A. Data model

Brain electrical activities are generated by the current flows that are associated with the transmission of information between neurons. In order to capture and measure these activities using surface EEG electrodes, a certain number of synchronized active neuronal populations is required. These brain electrical currents can be modeled using a grid of current dipoles forming the source space. Specifically, these neurons are oriented perpendicularly to the cortical surface [17]. Assume now that (i) T time samples of surface EEG signals have been collected using N_e surface scalp electrodes and stored in the space-time observation matrix $\boldsymbol{X} \in \mathbb{R}^{N_e \times T}$ and (ii) N_d source signals representing the activities of the N_d electrical dipoles constituting the source space are encoded in the signal matrix $\boldsymbol{S} \in \mathbb{R}^{N_d \times T}$. Assume also that the source space can be divided into two sub-spaces, the one corresponding to P extended sources that are responsible for the generation of the events of interest and the one containing the rest of grid dipoles. Note that an extended source stands for the union contiguous areas (patches) of cortex with highly electrical dipoles of synchronized activities. The observed EEG data can then be modeled as a linear mixture of the source signals as follows:

$$\boldsymbol{X} \approx \boldsymbol{G}\boldsymbol{S} = \sum_{k \in \Omega_e} \boldsymbol{g}_k \boldsymbol{s}_k^\intercal + \sum_{\ell \in \Omega_b} \boldsymbol{g}_\ell \boldsymbol{s}_\ell^\intercal \quad (3)$$

where the mixing operator $\boldsymbol{G} = [\boldsymbol{g}_1, \cdots, \boldsymbol{g}_{N_d}] \in \mathbb{R}^{N \times N_d}$ stands for the lead-field matrix which characterizes the attenuation inflected on the dipole signals before being measured by the surface scalp electrodes. Besides, vectors $\boldsymbol{g}_k$ and $\boldsymbol{s}_k$ stand respectively for the lead-field vector associated to the kth grid dipole and the kth row of $\boldsymbol{S}$. The set $\Omega_e = \cup_{p=1}^{P} \Omega_p, P << N_e$ denotes the set of indices of all grid dipoles involved in the generation of the events of interest with Ω_p being the set of indices of all grid dipoles constituting the pth epileptic patch. As far as the set Ω_b is concerned, it contains the indices of grid dipoles contributing to the generation of normal brain activity, well-known as background activity.

B. The All-in-One method

According to equation (3), solving the inverse problem in EEG consists in estimating the source matrix, $\boldsymbol{S}$, using the assumed known matrices $\boldsymbol{X}$ and $\boldsymbol{G}$. As the number of epileptic grid dipoles to be estimated is generally higher than the number of surface EEG electrodes, the EEG inverse problem is ill-posed and hence should be regularized to restore its identifiability. A natural approach to solve the regularized EEG inverse problem consists then in finding the solution, $\hat{\boldsymbol{S}}$, in a least squares sense as follows:

$$\hat{\boldsymbol{S}} = \arg\min_{\boldsymbol{S}} |||\boldsymbol{X} - \boldsymbol{G}\boldsymbol{S}||_F^2 + \sum_{c=1}^{C} \lambda_c f_c(\boldsymbol{S}) \tag{4}$$

where different prior informations on the target sources are encoded in the regularization terms $f_c(\boldsymbol{S})$ and $\lambda_c \in \mathbb{R}^*, 1 \leq c \leq C$ is the cth regularization parameter. It is note worthy that some EEG inverse problem methods consider only one time sample rather than the entire temporal structure of the data. For those methods, the data matrix $\boldsymbol{X}$ and the source matrix $\boldsymbol{S}$ are replaced in the above optimization problem (4) by the column vectors $\boldsymbol{x}$ and $\boldsymbol{s}$, respectively. Several assumptions on the target sources can be used to design f_c, such as minimum energy [9], [18], sparsity [19], [20], smoothness, etc. In this POC study, the assumption of sources of minimum energy is considered as initially proposed in [9]. Besides, EEG signals are well qualified as graph signals as brain activities can be mapped on a graph (network) with nodes corresponding to cortical grid dipoles and edges reflecting the functional coherence/synchronization between these nodes. Furthermore, as the activity of each epileptic patch is induced by hyper-synchronized activities of the patch's grid-dipoles, patch activity is, according to Definition 5, a smooth signal on graph. This smoothness measure is, according to equation (2), governed by the graph (normalized) Laplacian matrix which is to be learned here. Thus, based on the assumptions of sources of minimum energy and smooth on graph, the proposed AiOMNE approach addresses the following optimization problem:

$$\begin{aligned} \underset{\boldsymbol{S},\boldsymbol{L},\boldsymbol{D}}{\text{minimize}} \, & \|\boldsymbol{X} - \boldsymbol{G}\boldsymbol{S}\|_F^2 + \lambda_1 \|\boldsymbol{B}\boldsymbol{S}\|_F^2 + \lambda_2 \|\tilde{\boldsymbol{L}}^{1/2}\boldsymbol{S}\|_F^2 \\ & \qquad + \lambda_3 \|\tilde{\boldsymbol{L}}\|_F^2 \\ & \text{s.t. } \tilde{\boldsymbol{L}} = \boldsymbol{D}^{-1/2}\boldsymbol{L}\boldsymbol{D}^{-1/2} \\ & L_{i,j} < 0,\ 1 \leq i \neq j \leq N_d, \boldsymbol{L}\boldsymbol{1}_{N_d} = 0 \end{aligned} \tag{5}$$

where $\boldsymbol{B}$ is a diagonal weight matrix with $B_{d,d} = \|\boldsymbol{g}_d\|_2^{-1}$, $1 \leq d \leq N_d$ as suggested initially in the wMNE algorithm [9] with $\boldsymbol{g}_d$ denoting the dth column vector of $\boldsymbol{G}$. The additional regularization term $\|\tilde{\boldsymbol{L}}\|_F^2$ controls the distribution of graph edge weights [11]. Regarding the other regularization terms, $||\boldsymbol{B}\boldsymbol{S}||_F^2$ and $||\tilde{\boldsymbol{L}}^{-1/2}\boldsymbol{S}||_F^2$, they respectively encode the minimum energy and the smoothness on graph assumptions of the target epileptic sources. Solving the above optimization problem is performed iteratively in an alternative way. More precisely, at each iteration, each variable is computed while keeping the other one fixed to its last estimate. Then, by looking for the stationary points of the above cost function in both $\boldsymbol{S}$ and $\tilde{\boldsymbol{L}}$ with $\tilde{\boldsymbol{L}} = \boldsymbol{D}^{-1/2}\boldsymbol{L}\boldsymbol{D}^{-1/2}$, a closed form solution of $\boldsymbol{S}$ and $\boldsymbol{L}$ is obtained:

$$\boldsymbol{S} = \boldsymbol{\Psi}^{-1}\boldsymbol{G}^\intercal(\mathbf{I}_{N_e} + \boldsymbol{G}\boldsymbol{\Psi}\boldsymbol{G}^\intercal)^{-1}\boldsymbol{X} \tag{6}$$

$$\boldsymbol{L} = \frac{-2\lambda_3}{\lambda_2}\boldsymbol{D}^{1/2}\boldsymbol{S}\boldsymbol{S}^\intercal\boldsymbol{D}^{1/2} \tag{7}$$

where $\boldsymbol{\Psi} = \lambda_1\boldsymbol{B}^\intercal\boldsymbol{B} + \lambda_2\boldsymbol{D}^{-1/2}\boldsymbol{L}\boldsymbol{D}^{-1/2}$. As far as the diagonal degree matrix $\boldsymbol{D}$ is concerned, it is computed by setting its ith diagonal element to the corresponding ith diagonal element of the estimated graph Laplacian matrix $\boldsymbol{L}$ (7). The negativity constraint on the off-diagonal elements of $\boldsymbol{L}$ is simply handled at each iteration by setting them to zero when their current estimates are positive. The algorithm stops when the relative error on the estimation of $\boldsymbol{L}$ exhibits between two successive iterations a value that is smaller or equal to a predefined threshold or when the the maximum number of iterations is reached.

IV. Numerical results

The performance of the proposed algorithm is assessed on realistic simulated interictal epileptic EEG data (epileptiform spike) and compared to the classical sequential scheme using either wMNE or sLORETA methods. To this end, scalp epileptic EEG signals for $N_e = 91$ electrodes, $T = 200$ time instants at the sampling rate of 256 Hz are generated. The employed source space is composed of $D = 19626$ grid dipoles located on the cortical surface. The lead-field matrix is generated using the ASA software (ASA, ANT, Enschede, Netherlands) and a realistic head model composed of three compartments representing the brain, the skull, and the scalp. We consider two epileptic patches. One patch located on the Inferior Frontal gyrus (InfFr) and another patch on the Occipital-Temporal gyrus (OccTe). Each patch includes 100 grid dipoles corresponding to a cortical area of approximately $5cm^2$. Gaussian background activity is attributed to all grid dipoles outside the two epileptic patches. The amplitude of the background activity is adjusted to the amplitude of the depth EEG signals to get a realistic Signal to Noise Ratio (SNR) that verifies $||\boldsymbol{G}\boldsymbol{S}||_F/||\boldsymbol{\Xi}||_F \approx 1$ where $\boldsymbol{\Xi} \in \mathbb{R}^{N\times T}$ denote the noise matrix. Regularization parameters λ_1, λ_2 and λ_3 are automatically selected from a range of tested values based on a heuristic criterion. Retained values of λ_1, λ_2 and λ_3 are $70, 60$ and 20, respectively. To assess the performance of the two considered source imaging approaches, their respective localization accuracy is evaluated in terms of the Dipole Localization Error (DLE) [21] criterion:

$$\text{DLE} = \frac{1}{2Q}\sum_{k\in\mathcal{I}} \min_{\ell\in\hat{\mathcal{I}}} ||\boldsymbol{r}_k - \boldsymbol{r}_\ell||_2 + \frac{1}{2\hat{Q}}\sum_{\ell\in\hat{\mathcal{I}}} \min_{k\in\mathcal{I}} ||\boldsymbol{r}_k - \boldsymbol{r}_\ell||_2$$

where $\mathcal{I}$ and $\hat{\mathcal{I}}$ denote the original and the estimated sets of indices of all dipoles belonging to an active patch, Q and $\hat{Q}$ are the numbers of original and estimated active dipoles, and $\boldsymbol{r}_k$ denotes the position of the k-th source dipole. To

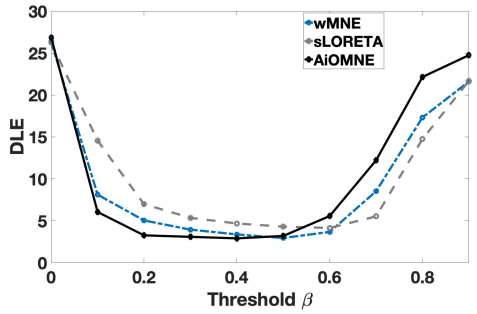

Fig. 1. DLE of wMNE, sLORETA and AiOMNE methods for different threshold values β.

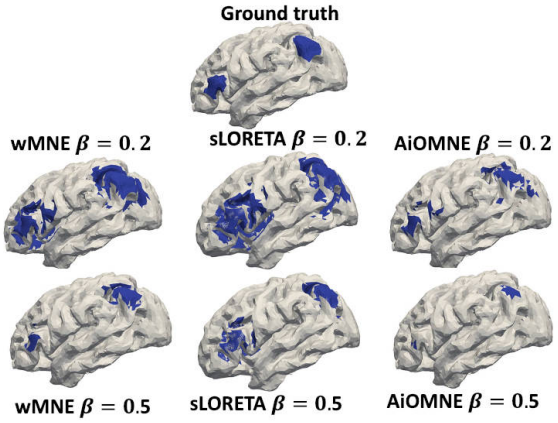

Fig. 2. Brain source localization by wMNE, sLORETA and AiOMNE for two threshold values $\beta = 0.2$ and $\beta = 0.5$.

determine the estimated sets of active dipoles for the single-step approach, we threshold the amplitudes of the estimated source distributions.

The DLE is averaged over 30 realizations of noisy EEG signals. More precisely, to compare the estimated source configuration to the ground truth, we consider a number of active estimated dipoles that is equal or as close as possible to the one of the true patch dipoles. To this end, a suitable threshold β is applied to the absolute value of AiOMNE, wMNE and sLORETA solutions. Figure 1 shows the localization accuracy of wMNE, sLORETA and AiOMNE in terms of DLE as a function of the threshold β which varies between 0.1 and 0.9. Globally when the adequate threshold is chosen for each method, a quasi-equivalent performance of the three methods is to be noticed. In this case, the best DLE values are equal to $2.91, 4.15$ and 2.95 for AiOMNE, sLORETA and wMNE, respectively. Besides, it can also be noted that contrary to wMNE and sLORETA where a relatively high threshold (i.e. $\beta = 0.5$) is to be considered for a good localization results of the two patches, the proposed AiOMNE method seems to be more effective for lower threshold (i.e., $\beta = 0.2$). This suggests that, contrary to wMNE and sLORETA which generally lead to blurred source localization results, the solution provided by AiOMNE is to some extent more accurate. This is confirmed in Figure 2 which illustrates, for two different thresholds $\beta = 0.2$ and $\beta = 0.5$, an example of source localization using wMNE, sLORETA and AiOMNE methods. Clearly, the reconstructed sources with wMNE and sLORETA for $\beta = 0.2$ are blurred. In addition, in the case of $\beta = 0.5$, even if the solution obtained by AiOMNE is sparse, it should be noticed that the barycentres of the two estimated patches coincide with the ground truth. To further assess the similarity between the estimated network and the ground truth, binary connectivity maps associated to the three considered methods are presented in Figure 3. Regarding the connectivity maps related to wMNE and sLORETA algorithms, shown in Figure 3, each of them stands for a binary representation of its associated correlation matrix that is computed using the reconstructed neural activities of the localized two patches (see Figure 2). As far as the connectivity map related to the proposed AiOMNE approach is concerned, it represents

TABLE I
HD BETWEEN BINARY CONNECTIVITY MAPS OF WMNE, SLORETA, AIOMNE AND THE GROUND TRUTH FOR TWO THRESHOLD VALUES $\beta = 0.2$ AND $\beta = 0.5$.

	Hamming Distance (HD)		
	wMNE	sLORETA	AiOMNE
$\beta = 0.2$	0.0015	0.0046	0.0001
$\beta = 0.5$	0.0001	0.0003	0.0001

also a binary representation of the graph adjacency matrix that is derived from the estimated graph Laplacian one. To create the binary connectivity map, a specific threshold is applied to the correlation/adjacency matrix. This threshold is determined by a predefined percentage of the highest value in the matrix. If an entry in the matrix has a value lower than this threshold, it is set to zero. Conversely, if the value is equal to or greater than the threshold, it is set to one. Once the binary matrices are computed, the similarity between an estimated connectivity and the one of the ground truth is computed using Hamming Distance (HD), for the two threshold values $\beta = 0.2$ and $\beta = 0.5$. The obtained results, as shown in Table I, demonstrate that the proposed AiOMNE method exhibits higher similarity in terms of connectivity patterns with the ground truth compared to wMNE and sLORETA, regardless of the employed threshold. According to Table I, the AiOMN algorithm exhibits significant improvements in terms of HD (Hamming Distance) compared to sLORETA and wMNE. Specifically, for $\beta = 0.2$, the AiOMNE method shows an improvement of approximately 46 times over sLORETA and around 14 times over wMNE. Similarly, for $\beta = 0.5$, the AiOMNE method demonstrates an improvement of about 4 times over sLORETA and around 2 times over wMNE in terms of HD.

The agreement between the DLE results and the previously mentioned findings further substantiates the superiority of the proposed AiOMNE method. It consistently achieves a higher similarity with the ground truth, even when utilizing a relatively small threshold value of $\beta = 0.2$.

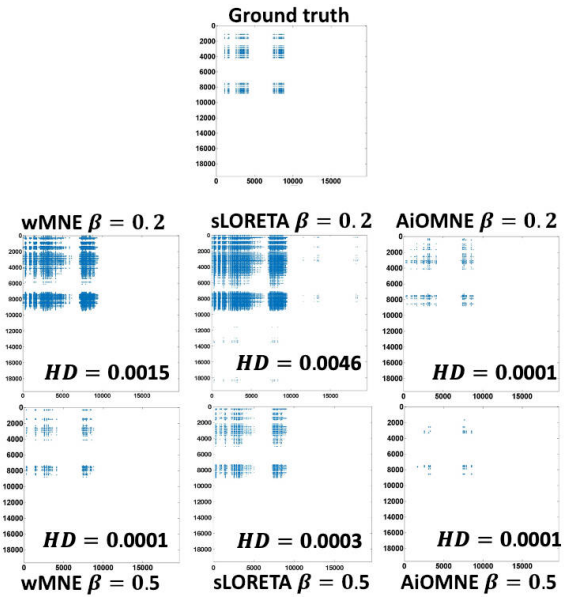

Fig. 3. Binary connectivity maps obtained by the sequential strategy where wMNE and sLORETA being used in the source localization step and AiOMNE, for different threshold values β and their respective Hamming Distance (HD) to the ground truth.

V. Conclusion

In this paper, a proof of concept study on solving simultaneously both the inverse problem in EEG and the inference of brain functional connectivity in the context of drug-resistant epilepsy was proposed. The new proposed approach, named AiOMNE, relies on the physiological assumption that epileptic EEG signals are smooth signals on graph. More precisely, the AiOMNE revisits the conventional wMNE approach by incorporating the smoothness on graph assumption as an additional regularization term. Preliminary results on realistic synthetic EEG data confirmed that the AiOMNE solution (i) attenuates the well-known blurred source localization problem which is inherent to wMNE leading to a more focal source localization solutions compared to wMNE and sLORETA methods and (ii) provides a relatively good estimation of brain functional connectivity.

References

[1] U. Braun, A. Schäfer, H. Walter, S. Erk, N. Romanczuk-Seiferth, L. Haddad, J. I. Schweiger, O. Grimm, A. Heinz, H. Tost, A. Meyer-Lindenberg, and D. S. Bassett, "Dynamic reconfiguration of frontal brain networks during executive cognition in humans," *Proceedings of the National Academy of Sciences*, vol. 112, no. 37, pp. 11 678–11 683, 2015.

[2] V. Sakkalis, "Review of advanced techniques for the estimation of brain connectivity measured with eeg/meg," *Computers in biology and medicine*, vol. 41, pp. 1110–7, 07 2011.

[3] O. Sporns, D. R. Chialvo, M. Kaiser, and C. C. Hilgetag, "Organization, development and function of complex brain networks," *Trends in Cognitive Sciences*, vol. 8, no. 9, pp. 418–425, 2004. [Online]. Available: https://www.sciencedirect.com/science/article/pii/S1364661304001901

[4] O. Sporns, *Networks of the brain*. MIT press, 2010.

[5] K. J. Friston, "Functional and effective connectivity in neuroimaging: A synthesis," *Human Brain Mapping*, vol. 2, no. 1-2, pp. 56–78, 1994. [Online]. Available: https://onlinelibrary.wiley.com/doi/abs/10.1002/hbm.460020107

[6] O. Sporns, G. Tononi, and K. Rolf, "The human connectome: A structural description of the human brain," *PLoS computational biology*, vol. 1, p. e42, 10 2005.

[7] P. A. Chantal, A. Karfoul, A. Nica, and R. L. B. Jeannès, "Dynamic brain effective connectivity analysis based on low-rank canonical polyadic decomposition: application to epilepsy," *Medical and Biological engineering and Computing*, vol. 59, pp. 1081–1098, 2015.

[8] M. Hassan, I. Merlet, A. Mheich, A. Kabbara, A. Biraben, A. Nica, and F. Wendling, "Identification of interictal epileptic networks from dense-eeg," *Brain Topography*, vol. 60, pp. 60–76, 2017.

[9] R. D. Pascual-Marqui, C. M. Michel, and D. Lehmann, "Low resolution electromagnetic tomography: A new method for localizing elecrical activity in the brain," *Int. Journal of Psychophysiology*, vol. 18, pp. 49 – 65, 1994.

[10] H. Becker, A. Karfoul, L. Albera, R. Gribonval, J. Fleureau, P. Guillotel, A. Kachenoura, L. Senhadji, and I. Merlet, "Tensor decomposition exploiting structural constraints for brain source imaging," in *2015 IEEE 6th International Workshop on Computational Advances in Multi-Sensor Adaptive Processing (CAMSAP)*, 2015, pp. 181–184.

[11] C. HU, L. Cheng, J. Sepulcre, K. A. Johnson, G. E. Fakhri, Y. M. Lu, and Q. Li, "A spectral graph regression model for learning brain connectivity of alzheimer disease," *PLoS ONE*, vol. 10, no. 5, pp. 128 – 136, 2015.

[12] X. Dong, D. Thanou, M. Rabbat, and P. Frossard, "Learning graphs from data: A signal representation perspective," *IEEE Signal Processing Magazine*, vol. 36, no. 3, pp. 44–63, 2019.

[13] R. D. Pascual-Marqui, "Standardized low resolution brain electromagnetic tomography (sLORETA): technical details," *Methods and Findings in Experimental and Clinical Pharmacology*, 2002.

[14] D. I. Shuman, S. K. Narang, P. Frossard, A. Ortega, and P. Vandergheynst, "The emerging field of signal processing on graphs: Extending high-dimensional data analysis to networks and other irregular domains," *IEEE Signal Processing Magazine*, vol. 30, no. 3, pp. 83–98, 2013.

[15] F. R. K. Chung, *Spectral Graph Theory*. American Mathematical Society, 1997.

[16] A. J. Smola and R. Kondor, "Kernels and regularization on graphs," in *Learning Theory and Kernel Machines*, B. Schölkopf and M. K. Warmuth, Eds. Berlin, Heidelberg: Springer Berlin Heidelberg, 2003, pp. 144–158.

[17] A. M. Dale and M. I. Sereno, "Improved localization of cortical activity by combining EEG and MEG with MRI cortical surface reconstruction: a linear approach," *Journal of Cognitive Neuroscience*, vol. 5, no. 2, pp. 162–176, 1993.

[18] E. Ou, M. Hämäläinen, and P. Golland, "A distributed spatio-temporal EEG/MEG inverse solver," *NeuroImage*, vol. 44, 2009.

[19] K. Uutela, M. Hämäläinen, and E. Somersalo, "Visualization of magnetoencephalographic data using minimum current estimates," *NeuroImage*, vol. 10, pp. 173 – 180, 1999.

[20] A. Gramfort, M. Kowalski, and M. Hämäläinen, "Mixed-norm estimates for the M/EEG inverse problem using accelerated gradient methods," *Physics in Medicine and Biology*, vol. 57, pp. 1937 – 1961, 2012.

[21] J.-H. Cho, S. B. Hong, Y.-J. Jung, H.-C. Kang, H. D. Kim, M. Suh, K.-Y. Jung, and C.-H. Im, "Evaluation of algorithms for intracranial EEG (iEEG) source imaging of extended sources: feasibility of using (iEEG) source imaging for localizing epileptogenic zones in secondary generalized epilepsy," *Brain Topography*, no. 24, pp. 91–104, 2011.